2mu4

NASA TECHNICAL NOTE

NASA TN D-7366

D-7366

MEAN FLOW AND TURBULENCE MEASUREMENTS IN A MACH 5 FREE SHEAR LAYER

by Richard D. Wagner

Langley Research Center
Hampton, Va. 23665

NATIONAL AERONAUTICS AND SPACE ADMINISTRATION • WASHINGTON, D. C. • DECEMBER 1973

1. Report No.	2. Government Accession No.	3. Recipient's Catalog No.
NASA TN D-7366		

4. Title and Subtitle	5. Report Date
MEAN FLOW AND TURBULENCE MEASUREMENTS IN A MACH 5 FREE SHEAR LAYER	December 1973
	6. Performing Organization Code
7. Author(s)	8. Performing Organization Report No.
Richard D. Wagner	L-9007
	10. Work Unit No.
9. Performing Organization Name and Address	501-06-08-01
NASA Langley Research Center Hampton, Va. 23665	11. Contract or Grant No.
	13. Type of Report and Period Covered
12. Sponsoring Agency Name and Address	Technical Note
National Aeronautics and Space Administration Washington, D. C. 20546	14. Sponsoring Agency Code

15. Supplementary Notes

16. Abstract

A study of the time-averaged mean flow and the turbulence in a Mach 5 free turbulent shear layer has been performed. When the experimental data were reduced with the assumption of constant static pressure through the shear layer, the mean-velocity profile in similarity coordinates was in good agreement with the low-speed velocity profile. The intensities of the velocity fluctuations were about a factor of 2 lower than the low-speed measurements but with the maximum velocity fluctuations occurring in the same regions of the supersonic and low-speed shear layers. A large density fluctuation was observed in the outer part of the shear layer near the boundary of the shear layer and the potential core.

17. Key Words (Suggested by Author(s))	18. Distribution Statement
Shear layer Hypersonic flow Turbulent flow	Unclassified – Unlimited

19. Security Classif. (of this report)	20. Security Classif. (of this page)	21. No. of Pages	22. Price*
Unclassified	Unclassified	~~29~~ 32	Domestic, $3.00 Foreign, $5.50

*For sale by the National Technical Information Service, Springfield, Virginia 22151

MEAN FLOW AND TURBULENCE MEASUREMENTS IN A MACH 5 FREE SHEAR LAYER

Richard D. Wagner
Langley Research Center

SUMMARY

A study of the time-averaged mean flow and the turbulence in a Mach 5 free turbulent shear layer has been performed. When the experimental data were reduced with the assumption of constant static pressure through the shear layer, the mean-velocity profile in similarity coordinates was in good agreement with the low-speed velocity profile. The intensities of the velocity fluctuations were about a factor of 2 lower than the low-speed measurements but with the maximum velocity fluctuations occurring in the same regions of the supersonic and low-speed shear layers. A large density fluctuation was observed in the outer part of the shear layer near the boundary of the shear layer and the potential core.

INTRODUCTION

The mechanics of free turbulent mixing attracts considerable interest because of its practical importance in the problems of aerodynamic jet noise and supersonic combustion. In each of these problems a detailed knowledge of both the time-averaged mean flow and the flow turbulence is required. Although progress has been made in the prediction of the time-averaged mean flow in free turbulent mixing problems (ref. 1), the capability for the prediction of the flow turbulence has not progressed correspondingly; the current theoretical approaches have relied by and large upon phenomenological models for the turbulent mixing. At present, the analytical and computational tools available to the theoretician appear to be inadequate to provide detailed knowledge of the flow turbulence, and experimental data are needed to guide future analytical developments.

The mechanics of free turbulent mixing at low speeds have been studied in detail and are well documented in the literature (refs. 2 and 3). Studies of free turbulent mixing in supersonic flow, where large density gradients in the flow may significantly alter the character of the turbulence, have been primarily limited to mappings of the time-averaged mean flow, and virtually no detailed information is available on the characteristics of the turbulence in supersonic free turbulent mixing. The results of the limited mean flow measurements (ref. 4) (such as, the greatly diminished spreading rate of the supersonic free turbulent shear layer) indicate that large differences may be expected between the low-speed and supersonic turbulence field in free shear layers.

The present paper reports the results of experiments conducted at the Langley Research Center to determine both the time-averaged mean flow and the flow turbulence in the near field of a Mach 5 free turbulent jet. The measurements were made by combining the results obtained in surveys of the jet shear layer with a pitot probe and a constant-current hot-wire anemometer.

SYMBOLS

A_w	overheat parameter
a	speed of sound
b	velocity difference half width, $y(u = u_e/2) - y(u = 0.95u_e)$
c	wire thermal capacity
D	nozzle-exit diameter
d	wire diameter
E'	finite-circuit parameter
e	wire voltage fluctuation
$f(M_l, M_e)$	nondimensional Mach number function
h	film coefficient of heat transfer
I	wire current
$K = \partial \log R_w / \partial \log T_w$	
k	thermal conductivity
L	wire length
M	Mach number
$\mathcal{M}$	time constant
m	mass flow
Nu_0	wire Nusselt number
P	wire power
p	static pressure
$p_{t,1}$	free-stream stagnation pressure
$p_{t,2}$	pitot pressure
R	gas constant
Re_x	Reynolds number
Re_0	wire Reynolds number

R_f	reference resistance
R_r	recovery resistance
R_w	wire resistance
R(M)	Rayleigh function
$R_{mT} = \overline{m'T_t'}/\tilde{m}\tilde{T}_t$	
$R_{\rho u} = \overline{\rho' u'}/\tilde{\rho}\tilde{u}$	
$R_{\sigma\tau} = \overline{\sigma'\tau'}/\tilde{\sigma}\tilde{\tau}$	
$r = \Delta e_m/\Delta e_t$	
T	flow temperature
T_f	reference temperature
T_r	recovery temperature
T_w	wire temperature
u	flow velocity, axial component
V	mean wire voltage
V_s	source velocity
v	flow velocity, transverse component
x,y	Cartesian coordinates
x_0	virtual origin
y*	translated y-coordinate
y_p	pressure trough edge
α_f	resistivity coefficient at T_f
α_r	resistivity coefficient at T_r
γ	specific-heat ratio
γ_f	nonlinear resistivity coefficient at T_f
γ_r	nonlinear resistivity coefficient at T_r
Δe_m	mass-flow sensitivity
Δe_t	total-temperature sensitivity
δ_p	shear-layer edge, potential core
ϵ	finite-circuit factor
η	recovery factor

μ	viscosity
ξ	similarity coordinate
ρ	density
σ	entropy perturbation
τ	vorticity perturbation
τ_{wr}	temperature loading

Superscripts:

$\sim$	root mean square (rms)
$-$	time-averaged value
$'$	instantaneous value

Subscripts:

e	shear-layer edge, potential core
l	local value
N_w	nozzle-wall value
r	recovery value
t	total condition

APPARATUS AND CALIBRATIONS

Test Facility

The measurements of the mean and fluctuating flow were taken in the near field of an adiabatic Mach 5 free jet that issued from a 10.6-cm-diameter nozzle. The nozzle was installed in the nozzle test apparatus at the Langley Research Center, and a schematic of the apparatus is shown in figure 1. The nozzle and jet were enclosed in a 61- by 61-cm vacuum chamber, and the jet exhausted into a diffuser approximately 42 cm downstream of the nozzle exit. An auxiliary air supply was used to bleed air into the vacuum chamber and, thereby, match the chamber and nozzle-exit static pressures. The nozzle-wall boundary layer was turbulent.

Instrumentation

The pitot probe was made of stainless-steel tubing, which was flattened and ground at the tip, so that the tip was 0.165 cm wide and about 0.25 mm across the flats. The wall thickness at the tip was about 0.063 mm. Since the shear layer at the survey station

(x = 26.7 cm) was about 2 cm thick, the shear-layer—to—probe-tip thickness ratio was large and should have a negligible effect on the measured pitot pressures.

The hot-wire system was a commercially available constant-current anemometer with a frequency response up to 500 kHz. The hot-wire probes consisted of two needles that were crimped into 0.32-cm-diameter steel tubing with the needle ends insulated from the tubing by Teflon sleeves. The needle tips were spaced about 0.25 cm apart. Nickel-plated platinum wire was silver soldered across the needles. A central portion of the wire was etched to remove the nickel coating; the remaining platinum wire was 5 μm in diameter and about 0.75 mm long (an aspect ratio of about 150). About a quarter-circle slack was formed in this, the sensitive portion of the wire, to avoid strain-gage effects (ref. 5).

Hot-Wire Calibrations

All data to be discussed (with the exception of some experiments to look at the hot-wire signal spectra) were obtained with a single wire. This wire was first checked for strain-gage oscillations by placing it in a hypersonic flow which had sufficient turbulence to excite strain-gage oscillations; none were present. The wire was then oven calibrated to determine its resistance variation with temperature. The temperature dependence of the electrical resistance of platinum wire is accurately represented by (ref. 6)

$$R_w = R_f \left\{ 1 + \alpha_f (T_w - T_f) + \gamma_f \left[\alpha_f (T_w - T_f) \right]^2 \right\} \tag{1}$$

where R_f is the wire resistance at a reference temperature T_f (herein taken as 273 K), and α_f and γ_f are the temperature sensitivity coefficients. The temperature range of the calibration oven was insufficient to determine accurately γ_f, and the oven was used only to determine α_f. The value found agreed with that given by Morkovin (ref. 6), $\alpha_f = 3.8 \times 10^{-3}$ per K. The approximation that is suggested by Morkovin (ref. 6), $\gamma_f = -0.045$, was used.

After oven calibration, the wire was flow calibrated in the potential core of the Mach 5 nozzle for heating rate and recovery temperature variation with flow conditions. This calibration was used in the mean flow data reduction and in the calculations of the wire sensitivities for turbulence measurements.

For $M > 1.2$, the hot-wire Nusselt number $Nu_0 = hd/k_t$ and the hot-wire recovery factor $\eta = T_r/T_t$ are independent of Mach number and depend only on the flow Reynolds number $Re_0 = \rho u d/\mu_t$. The calibration of the wire used in the present study is shown in figure 2.

For the calibration range

$$Nu_0 = -0.08 + 0.55\sqrt{Re_0} \tag{2}$$

and

$$\eta = 0.95 + 0.155/\mathrm{Re}_0^{1.32} \tag{3}$$

To avoid time-consuming measurements of the hot-wire time constant at each hot-wire operating point, the procedure described in reference 5 was used to measure the wire heat capacity as part of the flow calibration, and the hot-wire signal compensation procedure of reference 5 was used; that is, the hot-wire heat capacity was determined from the equation developed by Morkovin (ref. 6)

$$c = (\alpha_r R_r / A_w)\mathcal{M} I^2 (1 + 2 A_w \epsilon) / [1 - 2\gamma_r (R_w - R_r)/R_r] \tag{4}$$

where A_w is Morkovin's overheat parameter $A_w = \frac{1}{2}(\partial \log R_w / \partial \log I)$, I is the hot-wire current, ϵ is the finite-circuit factor, and $\mathcal{M}$ is the hot-wire time constant. As part of the flow calibration, at each Re_0, the wire time constant was found at one current by the square-wave heating technique and c was calculated from equation (4). An average of the resulting heat capacities (which were the same to within ± 5 percent) was used to calculate the hot-wire time constants from equation (4) for operating conditions in the shear-layer experiments. In the shear-layer experiments a single value of the time constant was set into the compensating amplifier at all currents and the rms data were corrected with the formula

$$\tilde{e}_{true} / \tilde{e}_{amp} = \mathcal{M}_{true} / \mathcal{M}_{amp} \tag{5}$$

where $\tilde{e}_{true}$ is the rms voltage at the correct compensation time constant $\mathcal{M}_{true}$, and $\tilde{e}_{amp}$ is the rms voltage measured in the tests with the compensating amplifier set at $\mathcal{M}_{amp}$. This procedure leads to some signal distortion at low frequencies on the order of the wire rolloff frequency (always less than 500 Hz), but this effect should be negligible.

DATA REDUCTION

Mean Flow Measurements

In principle, the combination of mean measurements which were taken (pitot pressure, hot-wire power, and wire recovery temperature) is sufficient to determine all the flow properties in the shear layer. The calibration equations can be inverted to give

$$\mathrm{Re}_0 = 3.305\mathrm{Nu}_0^2 + 0.529\mathrm{Nu}_0 + 0.02117 \tag{6}$$

where $\mathrm{Nu}_0 = \alpha_r R_r (dP/dR_w)_r / (\pi L k_t)$ and $(dP/dR_w)_r$ is the power-resistance derivative at $R_w = R_r$, the wire resistance at zero current. Since $T_r = T_r(R_r)$ (see eq. (1)), then with equation (3)

$$T_t = T_r / (0.95 + 0.155/\mathrm{Re}_0^{1.32}) \tag{7}$$

(For convenience, in discussions of the mean flow measurements, the superscript bar is not used, and all quantities are time-averaged values.) If the hot-wire power is measured at several currents, $(dP/dR_w)_r$ and R_r can be found; then a simple iteration

scheme can be used to find Re_0 and T_t. Other flow variables can then be found. Since

$$\rho u = \frac{Re_0 \mu_t}{d} = \gamma \frac{pM}{a_t} \sqrt{1 + \frac{\gamma - 1}{2} M^2} \tag{8}$$

and $p/p_{t,2} = R(M)$, the Rayleigh pitot formula, it can be shown that

$$\frac{Re_0 \mu_t \sqrt{\gamma R T_t}}{dp_{t,2}} = \gamma R(M) M \sqrt{1 + \frac{\gamma - 1}{2} M^2} \tag{9}$$

By either graphical solution or by iteration the local Mach number can be found. The static pressure, density, and velocity can then be directly calculated. However, the right-hand side of equation (9) is a very weak function of Mach number above about $M = 2$, and small errors in the measured quantities can lead to large errors in the predicted Mach number. This condition is illustrated in figure 3 wherein equation (9) has been nondimensionalized with the shear-layer-edge conditions so that

$$\frac{p_{t,1,e} Re_{0,l} T_{t,l}^2 \left(T_{t,e} + 198.6\right)}{p_{t,2,l} Re_{0,e} T_{t,e}^2 \left(T_{t,l} + 198.6\right)} = \frac{M_l \sqrt{1 + 0.2M_l^2} \left(1 + 0.2M_e^2\right)^3 \left(\frac{7M_l^2 - 1}{6}\right)^{5/2}}{M_e \left(1.2M_l^2\right)^{7/2}} = f(M_l, M_e)$$

where the Sutherland viscosity law has been used. This shortcoming of the present method of determining the mean-flow variables has been previously noted by Morkovin (ref. 6) and is discussed further in a subsequent section herein.

Turbulence Measurements

With the thermal inertia of the hot wire accounted for in both the time-constant prediction and signal correction, as noted in the section entitled "Instrumentation," the basic hot-wire equation that shows the fundamental sensitivity of the hot wire to mass flow and total-temperature fluctuations is

$$e'/V = \Delta e_t \, T_t'/\overline{T}_t - \Delta e_m \, m'/\overline{m} \tag{10}$$

where e', T_t', and m' are the instantaneous fluctuations in the hot-wire voltage, the total temperature, and the mass flow, respectively; V, $\overline{T}_t$, and $\overline{m}$ are the time-averaged values. The hot-wire sensitivities are given by Morkovin (ref. 6) as

$$\left.\begin{aligned} \Delta e_m &= E' \left[A_w \, \partial \log Nu_0 / \partial \log Re_0 - \left(A_w / \tau_{wr}\right) \partial \log \eta / \partial \log Re_0\right] \\ \Delta e_t &= E' \left\{K + A_w \left[K - 1.86 + 0.76 \, \partial \log Nu_0 / \partial \log Re_0 - \left(0.76 / \tau_{wr}\right) \partial \log \eta / \partial \log Re_0\right]\right\} \end{aligned}\right\} \tag{11}$$

where the Mach number independence and appropriate constants for air have been inserted. The finite-circuit parameter is E', and the hot-wire temperature loading is $\tau_{wr} = (T_w - T_r)/T_r$.

As suggested by Kovásznay (ref. 7), modal analysis of the rms voltage fluctuations can be made by observing a virtual total-temperature fluctuation $\tilde{e}/(V\Delta e_t)$ at several sensitivity ratios $r = \Delta e_m/\Delta e_t$. From equation (10)

$$\left[\tilde{e}/(V\Delta e_t)\right]^2 = (\tilde{T}_t/\bar{T}_t)^2 - 2r(\tilde{T}_t/\bar{T}_t)(\tilde{m}/\bar{m})R_{mT} + r^2(\tilde{m}/\bar{m})^2 \tag{12}$$

where R_{mT} is the correlation coefficient for the mass flow and total-temperature fluctuations. To generate mode diagrams, the hot wire was operated through 7 to 10 currents; that is, 7 to 10 values of r. This procedure yields redundant information to determine the three unknowns, $\tilde{T}_t$, $\tilde{m}$, and R_{mT}.

TEST CONDITIONS

The jet shear layer was surveyed at a station 26.7 cm downstream of the nozzle exit. All tests were performed at a stagnation pressure and temperature of 79.3 N/cm^2 and 360 K, respectively. The corresponding unit Reynolds number was 0.175×10^6 per cm, or $Re_x = 4.68 \times 10^6$ based on the distance x from the nozzle exit to the survey station. The Mach number at the shear layer edge was 4.99.

To determine to what degree the flow at the survey station was a fully developed turbulent flow, reference to the results of Morrisette and Birch (ref. 4) is made. A result of their mapping of the mean flow (at the same stagnation pressure and temperature) is shown in figure 4 wherein lines of constant-velocity ratio are plotted against axial distance and Reynolds number. For $Re_x > 1.5 \times 10^6$, the data display the linear spreading that is often believed to be indicative of fully developed turbulent flow. However, measurements made by Morrisette and Birch (ref. 4) at a higher stagnation pressure also show linear spreading but at a lower spreading rate; they interpret this as an indication of incomplete development of the flow. While this conclusion is probably correct, for the present survey at $Re_x = 4.68 \times 10^6$, the local mean flow should be nearly fully developed; however, this may not assure full development of the turbulence field. To determine to what extent the flow turbulence is fully developed requires surveys and mappings of the flow turbulence beyond the intended scope of the present study.

RESULTS AND DISCUSSION

Mean Flow Measurements

The basic mean flow data obtained from the pitot probe and from iteration of the hot-wire data are shown in figure 5. The pitot-pressure and Re_θ profiles are similar,

with each displaying strong gradients near the shear-layer edge (high-velocity side). Near the shear-layer edge a slight overshoot above free-stream total temperature is observed in the total-temperature profile; deep in the shear layer the total temperature approaches the nozzle-wall temperature. Kistler (ref. 8) has measured similar overshoots in total temperature in the outer region of attached turbulent boundary layers and temperature deficits near the wall for $1.72 \leqq M \leqq 4.67$ and adiabatic walls. A total-temperature deficiency at an adiabatic wall is expected for air since the laminar Prandtl number is less than 1 and laminar transport is important near the wall. These data have been used to compute the Mach number function $f(M_l, M_e)$, and the profile of this function is shown in figure 6. Also shown in figure 6 are the distribution of $f(M_l, M_e)$ which would be obtained if the static pressure is assumed constant through the shear layer (equal to p_e) and a profile for a discontinuous static pressure: a static pressure trough with $p_l = p_e/2$ at the outer edge of the shear layer. Figure 6 illustrates the fundamental difficulty in attempting to use the present combination of variables to determine the mean flow properties. Because of the sensitivity of the Mach number to the combined measured variables, small errors in measured quantities on the order of ±5 percent can lead to differences in static pressure as great as 100 percent.

The cluster of data points from $\delta_p < y < y_p$ suggests that a trough in static pressure may exist in this region. The normal momentum equation for turbulent shear flows suggests that pressure gradients can occur in hypersonic turbulent shear flows because this equation states that (ref. 9)

$$\partial p/\partial y = -\partial\left(\rho\overline{v'^2}\right)\Big/\partial y$$

where v' is the normal-velocity component fluctuation. This equation can be integrated and nondimensionalized with the result

$$p_l/p_e = 1 - \gamma M_e^2 \left(\rho_l/\rho_e\right)\left(\overline{v'^2}/u_e^2\right)$$

Hence, if the turbulence intensity is not greatly diminished at high Mach numbers, then the Mach number squared factor would imply increasingly significant pressure variations in shear layers as M_e increases. Obviously, the present data do not have the precision needed to resolve whether static-pressure variations occur, and the data to be presented were reduced by assuming constant static pressure.

The mean velocity, density, and temperature profiles computed by assuming constant static pressure are shown in figure 7. Measurements were made to a point in the shear layer where the local Mach number had decreased to about 1. The subsonic and transonic portions of the shear layer were not surveyed since the hot-wire calibration becomes Mach number dependent therein. (Note that some error in the data point at $y \approx 3.0$ cm can be expected since the flow is transonic there.) Over the survey region a substantial density variation occurs with the density decreasing by about a factor of 5.

The velocity profile is again presented in figure 8, wherein the transverse coordinate has been redefined and nondimensionalized by the velocity defect half width of the shear layer, $b = y(u = u_e/2) - y(u = 0.95u_e)$. Therein, $\xi = y^*/b = \left[y(u = u_e/2) - y(u)\right]/b$. This nondimensionalization enables a comparison of the present hypersonic shear-layer velocity profile with the incompressible profile obtained by Liepmann and Laufer (ref. 10) which is also shown in figure 8. The linearized similarity solution (ref. 3), the error integral, is included in the figure. The two sets of experimental data agree quite well and thus indicate no appreciable effect of compressibility on the mean flow velocity profile in similarity coordinates. However the spreading-rate parameter σ for the compressible shear layer is about three times larger than the low-speed σ (see ref. 4); the compressible free shear layer spreads very slowly compared with the incompressible free shear layer. (The parameter σ is the constant in the similarity variable $\xi = \sigma y^*/(x - x_0)$ where x_0 is the virtual origin of the turbulent shear layer.)

Turbulence Measurements

Potential core.- A profile of the hot-wire virtual total-temperature fluctuations at 26.7 cm downstream of the exit is shown in figure 9. The data were taken from signal mode diagrams at hot-wire operating points corresponding to $r = 0.5$. At the boundary of the shear layer and the potential core, $y \approx 1$ cm, the hot-wire signal shows a rapidly increasing turbulence intensity with distance into the shear layer. In the potential core of the jet the turbulence intensity is nearly constant. To examine the nature of the turbulence in the potential core near the shear-layer edge, three mode diagrams of the hot-wire signals in the potential core are shown in figure 10: $x/D = 0$, $x/D = 1.45$, and $x/D = 2.54$. All three mode diagrams are linear. From equation (12) it follows that $R_{mT} = -1$, and the slopes of the mode diagrams give the rms of the mass flow fluctuations, and the intercepts $r = 0$ yield the rms of the total-temperature fluctuations; these quantities are listed in table I. The linear mode diagrams are consistent with the interpretation of the flow disturbances as being radiated sound (ref. 11). The analysis of Laufer (ref. 11) can be used to calculate the intensity of the sound $\tilde{p}/\bar{p}$, and this is included in table I.

TABLE I.- FLUCTUATION LEVELS IN POTENTIAL CORE

x/D	$\tilde{m}/\bar{m}$, %	$\tilde{T}_t/\bar{T}_t$, %	$\tilde{p}/\bar{p}$, %
0	1.12	0.08	2.16
1.45	3.34	.30	4.89
2.54	3.36	.12	4.79

The intensity of the sound radiated from the turbulent nozzle-wall boundary layer and sensed by the hot wire at the nozzle exit is about 2.5 times smaller than the sound intensity measured in the potential core downstream of the nozzle exit and presumably radiated from the free turbulent shear layer. The reason for this apparently more efficient radiation of sound is not known, but it may be due to an effective feedback possible through the low-speed flow on the low-velocity side of the shear layer. This higher intensity sound in the potential core downstream of the nozzle exit could be important in facilities with open jet test sections, particularly since the free-stream disturbance level has a strong influence on model boundary-layer transition locations.

Shear layer.- Mode diagrams of the hot-wire signals through the shear layer are shown in figure 11. For each diagram curves were faired through the data, and three points were taken from the fairings and used to calculate the coefficients of a quadratic fit so that

$$\left[\tilde{e}/(V\Delta e_t)\right]^e = C_1 r^2 + C_2 r + C_3 \tag{13}$$

The coefficients C_1, C_2, and C_3 were then used to compute $\tilde{m}/\overline{m}_l$, $\tilde{T}_t/\overline{T}_{t,l}$, and R_{mT} (see eq. (12)) which are shown in figure 12. The solid symbols and dashed-line curves in figure 11 are points and extensions of the mode diagrams obtained from equation (13) by using the coefficients C_1, C_2, and C_3.

Near the edge of the shear layer (high-velocity side) the mode diagrams were linear, as in the potential core, and hence $R_{mT} = -1$. Note that R_{mT} appears to change sign at about the location in the shear layer where $\overline{T}_t$ is a maximum (see fig. 5). Since m decreases monotonically into the shear layer, this change in sign of R_{mT} is suggestive of an eddy pattern where low T_t eddies on the high-velocity side of the shear-layer peak $\overline{T}_t$ are brought in with excess m (and vice versa), and the reverse occurs on the low-velocity side of the shear-layer peak $\overline{T}_t$. In this outer region the density gradient is a maximum (1 cm $< y <$ 1.5 cm), and the velocity gradient is small. By recalling the definition of total temperature, it follows that

$$\frac{T_t'}{\overline{T}_t} = \left(1 + \frac{\gamma - 1}{2} M^2\right)^{-1}\left[\frac{T'}{\overline{T}} + (\gamma - 1)M^2 \frac{u'}{\overline{u}}\right] \tag{14}$$

or for large M

$$\frac{T_t'}{\overline{T}_t} \approx \frac{2u'}{\overline{u}} \tag{15}$$

Since $\tilde{T}_t/\overline{T}_{t,l}$ is small in this outer region of the shear layer (less than 2 percent; see fig. 12), then the large mass flow fluctuations must consist predominantly of density fluctuations. However, it must be pointed out that equation (15) applies only for the T_t' that are not caused by a moving potential disturbance (see ref. 8 and subsequent equations). Some contribution to the fluctuations must come from the potential sound field radiated away from the shear layer, as previously discussed.

Farther into the shear layer the mass flow fluctuations reach a maximum intensity ($\tilde{m}/\bar{m}$ as high as about 17 percent) and the $\tilde{T}_t/\bar{T}_{t,l}$ increase to a maximum measured value of about 6 percent (see fig. 12). Where the total-temperature fluctuations become large, the mode diagrams become nonlinear with R_{mT} approaching 1; this is indicative of vorticity fluctuations becoming an important contribution to the disturbance patterns.

The resolution of the mass flow and total-temperature fluctuations into velocity and density fluctuations requires some assumption regarding the nature of the disturbances in the shear layer. Kovásznay (ref. 7) has argued that the expected fluctuations in shear flows should be primarily entropy and vorticity patterns; however, measurements of wall-pressure fluctuations under turbulent boundary layers and the radiated sound fields indicate that sound can become an important contributor to the turbulence field at high supersonic Mach numbers. Kistler (ref. 8) has examined the possible errors involved in neglecting the pressure fields, and Laderman and Demetriades (ref. 12) have attempted to obtain an estimate of the importance of pressure fluctuations in a boundary layer at M = 9.4 by including the assumption that

$$\frac{\tilde{p}}{\bar{p}_l} = \frac{\gamma M_l^2}{2}\left(\frac{\tilde{u}}{\bar{u}_l}\right)^2 \tag{16}$$

into the analysis of mode diagrams. They concluded that the pressure fluctuation terms were negligible. Equation (16) was used to estimate levels of pressure fluctuations that could be induced by the velocity fluctuations (which were calculated with the no-sound assumption) in the present work and the resulting possible $\tilde{p}/\bar{p}_l$ were indeed small (as shown subsequently). However, equation (16) omits the possibility of a sound pattern moving with some velocity relative to the mean flow, as occurs in the measured radiation field external to the shear layer. For example, with the hypersonic assumption, $M \gg 1$, the results of Kistler's analysis (ref. 8) (to determine the pressure and total-temperature fluctuations produced by a potential disturbance pattern moving with a velocity V_s and producing a velocity fluctuation u') can be written as

$$\frac{\tilde{p}}{\bar{p}_l} = \gamma M_l^2 \frac{\tilde{u}}{\bar{u}_l}\frac{\bar{u}_l - V_s}{\bar{u}_l} \tag{17}$$

and

$$\frac{\tilde{T}_t}{\bar{T}_{t,l}} = \frac{2\tilde{u}}{\bar{u}_l}\frac{V_s}{\bar{u}_l} \tag{18}$$

Obviously, unless $\bar{u}_l - V_s = O(u')$, equation (16) underestimates the pressure fluctuations. For example, if $V_s/\bar{u}_l \approx 0.5$ (see ref. 11) is assumed, and then the pressure fluctuations in the potential core are calculated by using equation (16) and $\tilde{T}_t/\bar{T}_{t,l} = 0.30$ percent (see table I), the $\tilde{p}/\bar{p}_l$ indicated would be about 0.06 percent; whereas equation (17) would give about 5 percent, or close to the correct value in table I.

Apparently, the present information is not sufficient to evaluate clearly the importance of possible pressure fluctuations, and a measurement of a third flow variable in addition to the hot wire $(\rho u)'$ and T_t' is needed. Nevertheless, further discussion of the present data proceeds on the assumption that the pressure fluctuations are of secondary importance.

The rms of the velocity and density fluctuations and the correlation coefficient are shown in figure 13. Note that with the assumption $p' = 0$, the velocity and density fluctuations are related to the vorticity and entropy fluctuations by $\tilde{\tau} = \tilde{u}/\bar{u}_l$ and $\tilde{\sigma} = \tilde{\rho}/\bar{\rho}_l$ (ref. 6). The density fluctuation in percent of the local density reaches a maximum of about 14 percent in the outer region of the shear layer adjacent to the potential core and where the mean-density gradients are large. Deeper in the shear layer (toward the low-velocity side) where the density gradients are small, the density fluctuations subside. A maximum velocity fluctuation in percent of local mean velocity is not obtained in the survey region; the velocity fluctuation intensity increases with depth into the shear layer. The correlation coefficient $R_{\rho u}$ changes abruptly from -1 to near 1 (about 0.85) in the shear layer. This change suggests that the density fluctuations in the part of the shear layer where $y > 1.5$ cm are driven by the velocity fluctuations, as has been previously observed in turbulent boundary-layer studies (ref. 8). Also shown in figure 13 are the pressure fluctuations (computed from eq. (16)) which appear small.

In figure 14 the velocity and density fluctuations (in percent of free-stream velocity and density) are again shown and may be compared with the measurements of Liepmann and Laufer (ref. 10) at low speeds. The maximum velocity fluctuation intensity measured by Liepmann and Laufer was about 15 percent and was located at about the point in the layer where $\bar{u}/\bar{u}_e \approx 0.5$ or $\xi = 0$; here the velocity gradient is about a maximum also. The present data indicate a maximum velocity fluctuation intensity also near $\xi = 0$, although measurements in the subsonic portion of the shear layer are needed for confirmation. For the present high Mach number shear layer, however, the intensity of the velocity fluctuations is much less, about a factor of 2 lower than in the low-speed shear layer. This result is consistent with the observed slower spreading of the $M_e = 5$ turbulent shear layer reported in reference 4. Therein, the experimentally determined spreading-rate parameter (that is, for the present shear layer) was $\sigma = 27$ compared with the low-speed value of about 11. Certainly, the diminished turbulence level should result in a lesser spreading rate or larger spreading-rate parameter. Kistler (ref. 8), in his study of supersonic turbulent boundary layers, has also observed a falloff of velocity fluctuation intensities with increasing Mach number. Gooderum, Wood, and Brevoort (ref. 13) carried out an experimental investigation into the conditions at the free boundary of a supersonic jet and also observed a narrower mixing zone and a level of turbulence somewhat smaller than in low-speed flow.

Signal spectra.- At three locations in the shear-layer survey, the hot-wire signal was recorded on a wide-band tape recorder, and these recordings were used to generate the signal spectra shown in figure 15. (The wire used in these measurements was not the one used in the surveys discussed thus far, and it had a small strain-gage oscillation at a frequency of about 180 kHz.) The three locations were: (1) At the edge of the shear layer in the potential core, $y^*/b \approx 2$; (2) at the point of peak density fluctuations, $y^*/b \approx 1$; and (3) near the point of peak velocity fluctuations, $y^*/b \approx 0.2$. The spectra of figure 15 are those of the recorded signal which included the instrumentation noise; the spectrum of the instrument noise is included in the figure. The frequency, which corresponds to eddies of size b, transported with a velocity u_e is also shown in the figure. Since b is about half the shear-layer thickness, clearly, in the shear layer most of the turbulence is governed by large-scale eddies, as occurs in attached turbulent shear layers (ref. 8). Very little energy in the spectrum is observed for frequencies corresponding to eddy sizes less than about one-third the layer thickness. In the potential core, $y^*/b \approx 2$, the spectrum contains even less energy in the high-frequency region than the spectrum of the signal in the shear layer from the radiation generating sources; Laufer first observed this deficit of energy at high frequency in studies of the radiation fields of attached turbulent boundary layers (ref. 14).

CONCLUDING REMARKS

A study of the time-averaged mean flow and the turbulence in a Mach 5 free turbulent shear layer has been performed. Because of the sensitivity of the predicted Mach number to the combination of variables measured, the present measurements were unable to determine whether static-pressure gradients exist in the hypersonic shear layer. However, reduction of the data with the assumption of constant static pressure led to a mean-velocity profile in similarity coordinates that was in good agreement with the low-speed profile. The intensities of the velocity fluctuations were about a factor of 2 lower than the low-speed measurements, but with the maximum velocity fluctuations occurring in the same regions of the supersonic and low-speed shear layers. A large density fluctuation was observed in the outer part of the shear layer near the boundary of the shear layer and the potential core.

Langley Research Center,
National Aeronautics and Space Administration,
Hampton, Va., August 30, 1973.

REFERENCES

1. Anon.: Free Turbulent Shear Flows. Vols. I and II. NASA SP-321, 1973.

2. Hinze, J. O.: Turbulence. McGraw-Hill Book Co., Inc., 1959.

3. Schlichting, Hermann (J. Kestin, transl.): Boundary-Layer Theory. Sixth ed., McGraw-Hill Book Co., Inc., 1968.

4. Morrisette, E. Leon; and Birch, Stanley F.: Mean Flow and Turbulence Measurements in a Mach 5 Shear Layer. Pt. I – The Development and Spreading of the Mean Flow. Fluid Mechanics of Mixing, Earl M. Uram and Victor W. Goldschmidt, eds., Amer. Soc. Mech. Eng., c.1973, pp. 79-86.

5. Wagner, R. D., Jr.; Maddalon, D. V.; Weinstein, L. M.; and Henderson, A., Jr.: Influence of Measured Free-Stream Disturbances on Hypersonic Boundary-Layer Transition. AIAA Paper No. 69-704, June 1969.

6. Morkovin, Mark V.: Fluctuations and Hot-Wire Anemometry in Compressible Flows. AGARDograph 24, Nov. 1956.

7. Kovásznay, Leslie S. G.: Turbulence in Supersonic Flow. J. Aeronaut. Sci., vol. 20, no. 10, Oct. 1953, pp. 657-674, 682.

8. Kistler, Alan L.: Fluctuation Measurements in a Supersonic Turbulent Boundary Layer. Phys. Fluids, vol. 2, no. 3, May-June 1959, pp. 290-296.

9. Lin, C. C., ed.: Turbulent Flows and Heat Transfer. Princeton Univ. Press, 1959.

10. Liepmann, Hans Wolfgang; and Laufer, John: Investigations of Free Turbulent Mixing. NACA TN 1257, 1947.

11. Laufer, John: Aerodynamic Noise in Supersonic Wind Tunnels, J. Aerosp. Sci., vol. 28, no. 9, Sept. 1961, pp. 685-692.

12. Laderman, A. J.; and Demetriades, A.: Measurements of the Mean and Turbulent Flow in a Cooled-Wall Boundary Layer at Mach 9.37. AIAA Paper No. 72-73, Jan. 1972.

13. Gooderum, Paul B.; Wood, George P.; and Brevoort, Maurice J.: Investigation With an Interferometer of the Turbulent Mixing of a Free Supersonic Jet. NACA Rep. 963, 1950. (Supersedes NACA TN 1857.)

14. Laufer, John: Sound Radiation From a Turbulent Boundary Layer. Tech. Rep. No. 32-119 (Contract No. NASw-6), Jet Propulsion Lab., California Inst. Technol., Nov. 1, 1961.

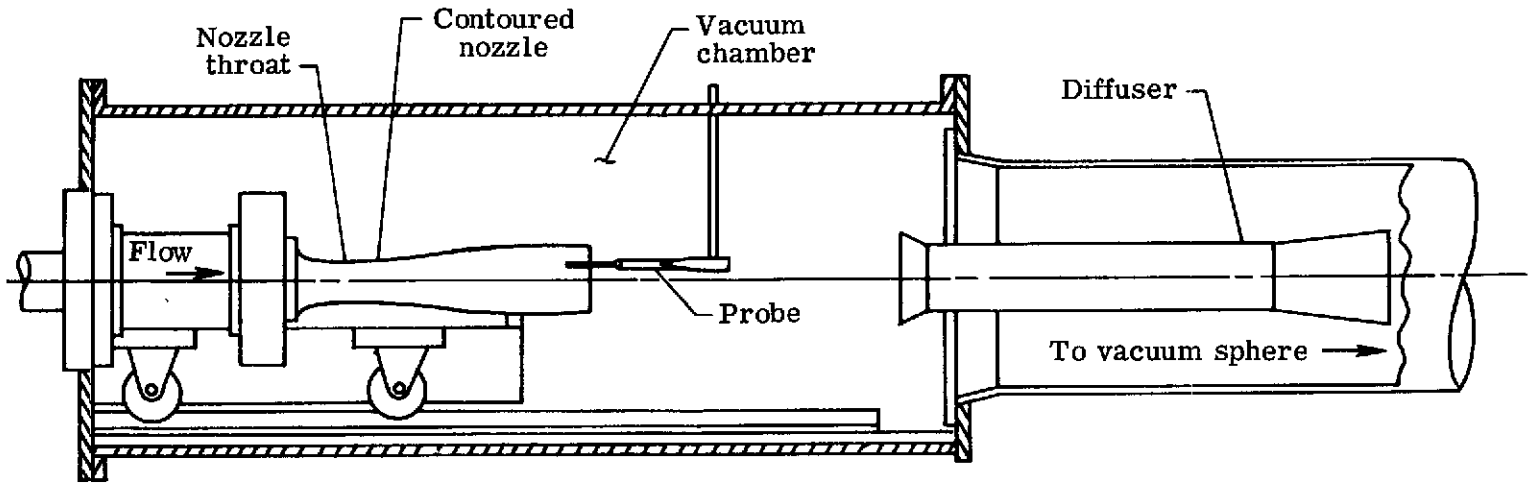

Figure 1.- Nozzle test chamber and Mach 5 nozzle.

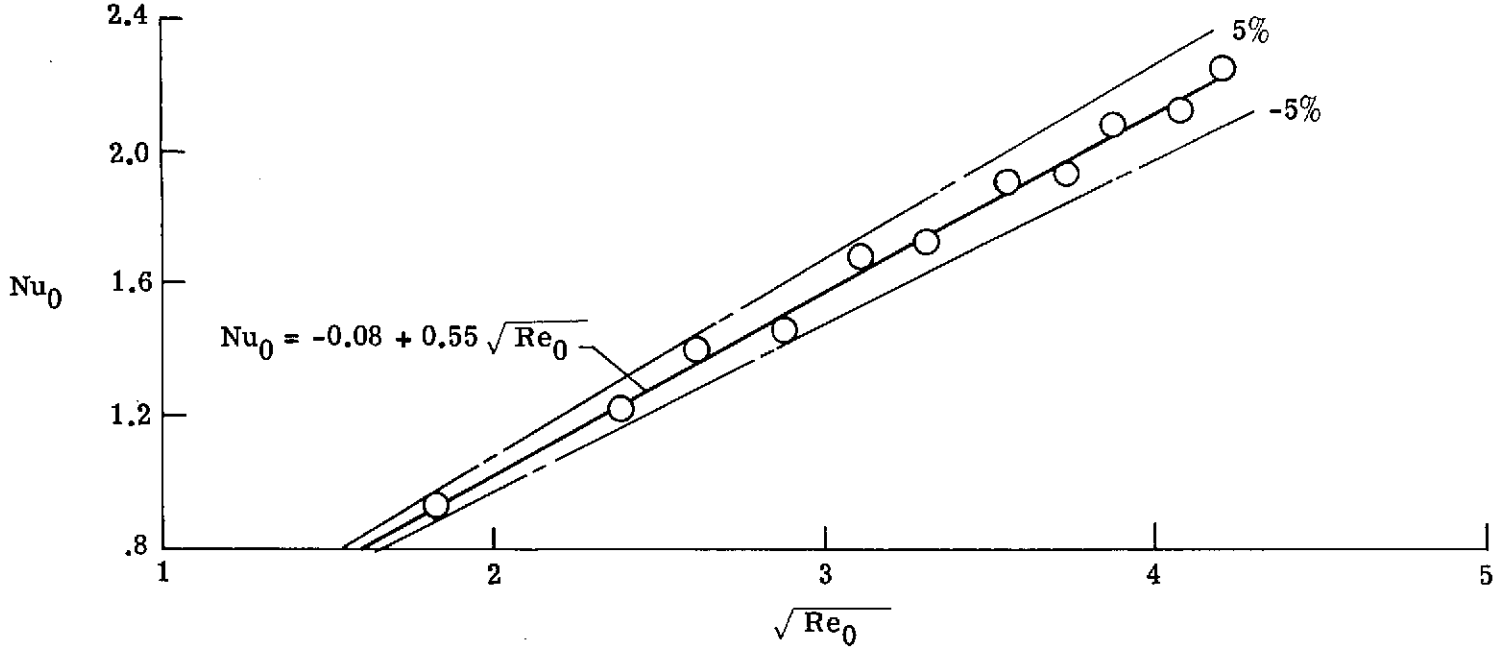

(a) Nusselt number.

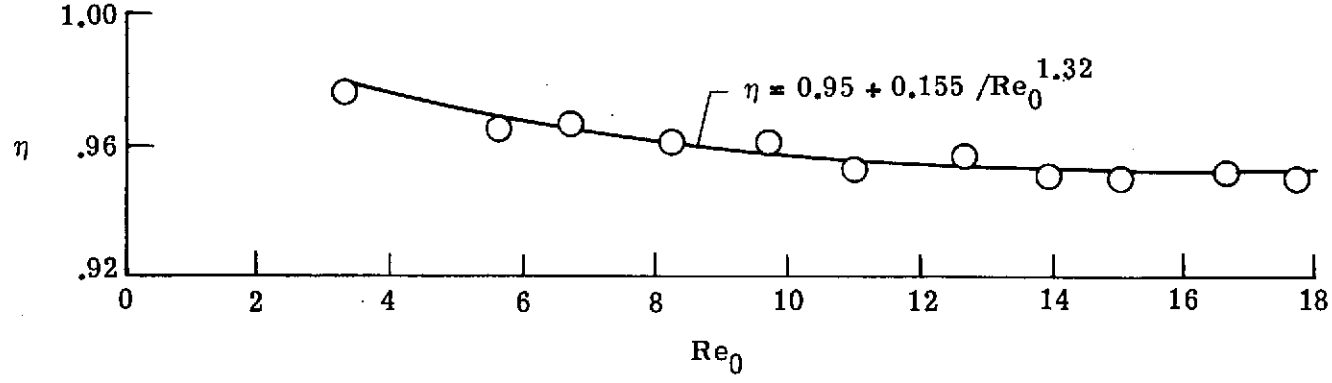

(b) Recovery factor.

Figure 2.- Hot-wire calibration.

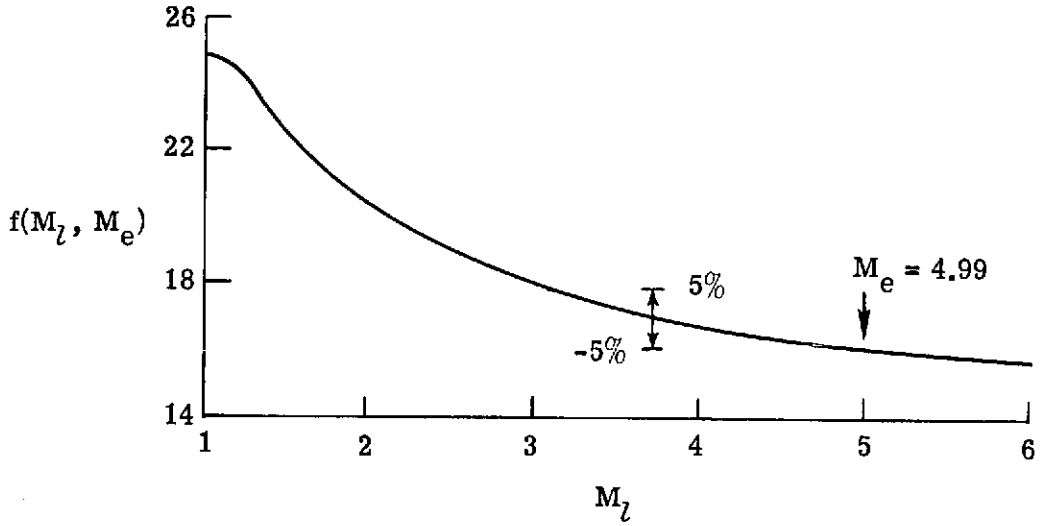

Figure 3.- Relationship of Mach number to measured flow quantities.

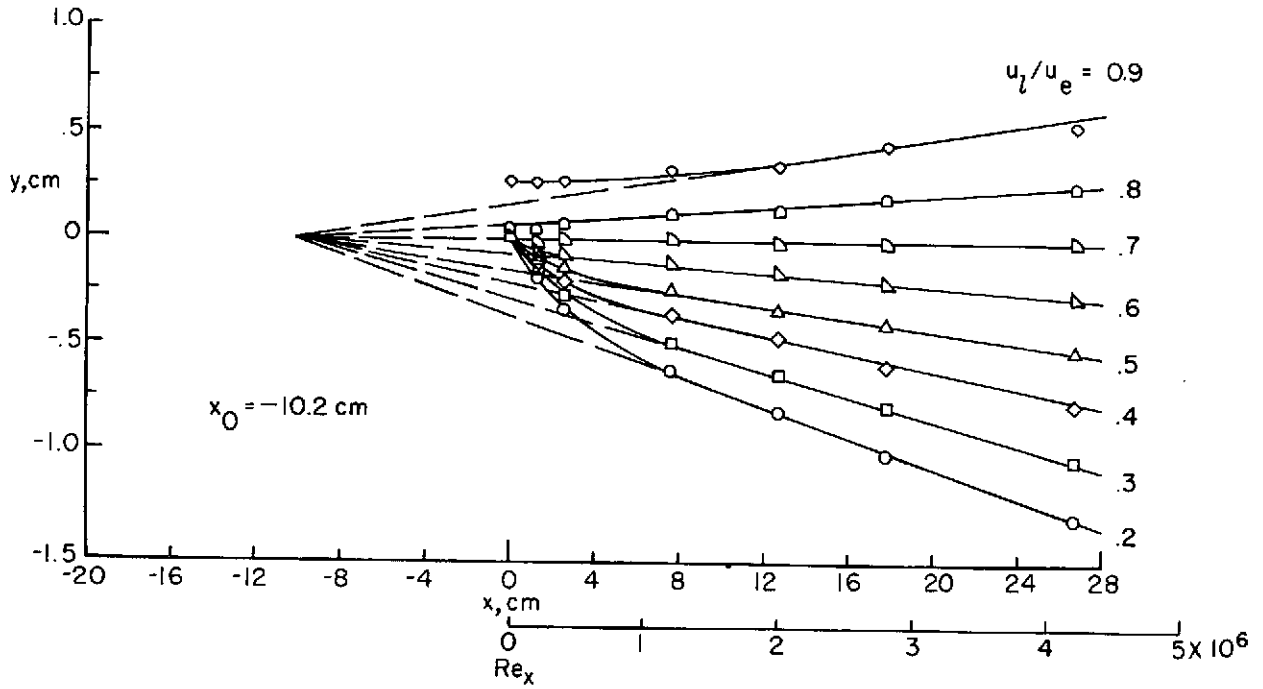

Figure 4.- Mean flow data lines of constant-velocity ratio (ref. 4).

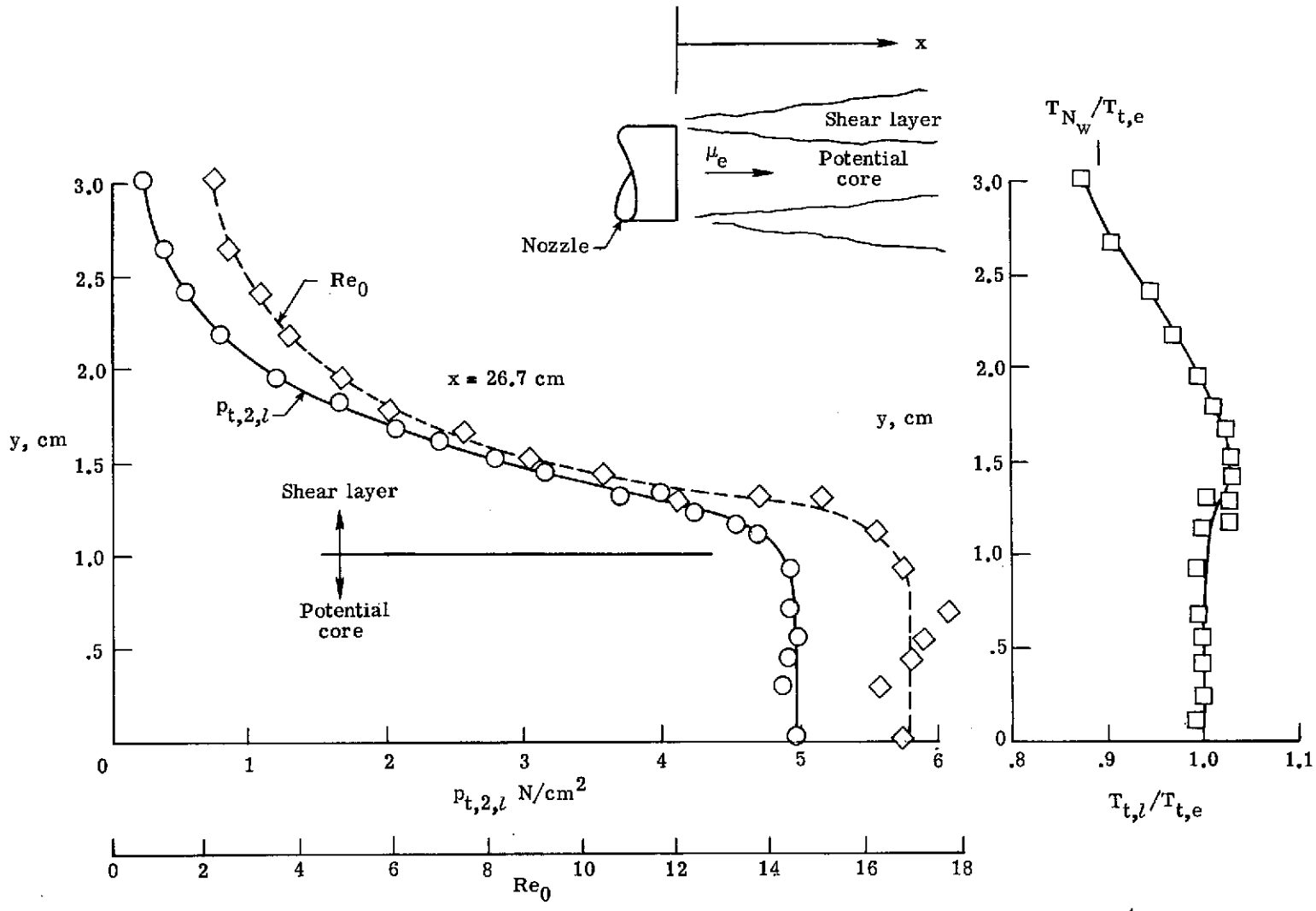

(a) $p_{t,2,\ell}$ and Re_0 profiles.

(b) $T_{t,\ell}/T_{t,e}$ profile.

Figure 5.- Basic mean flow data.

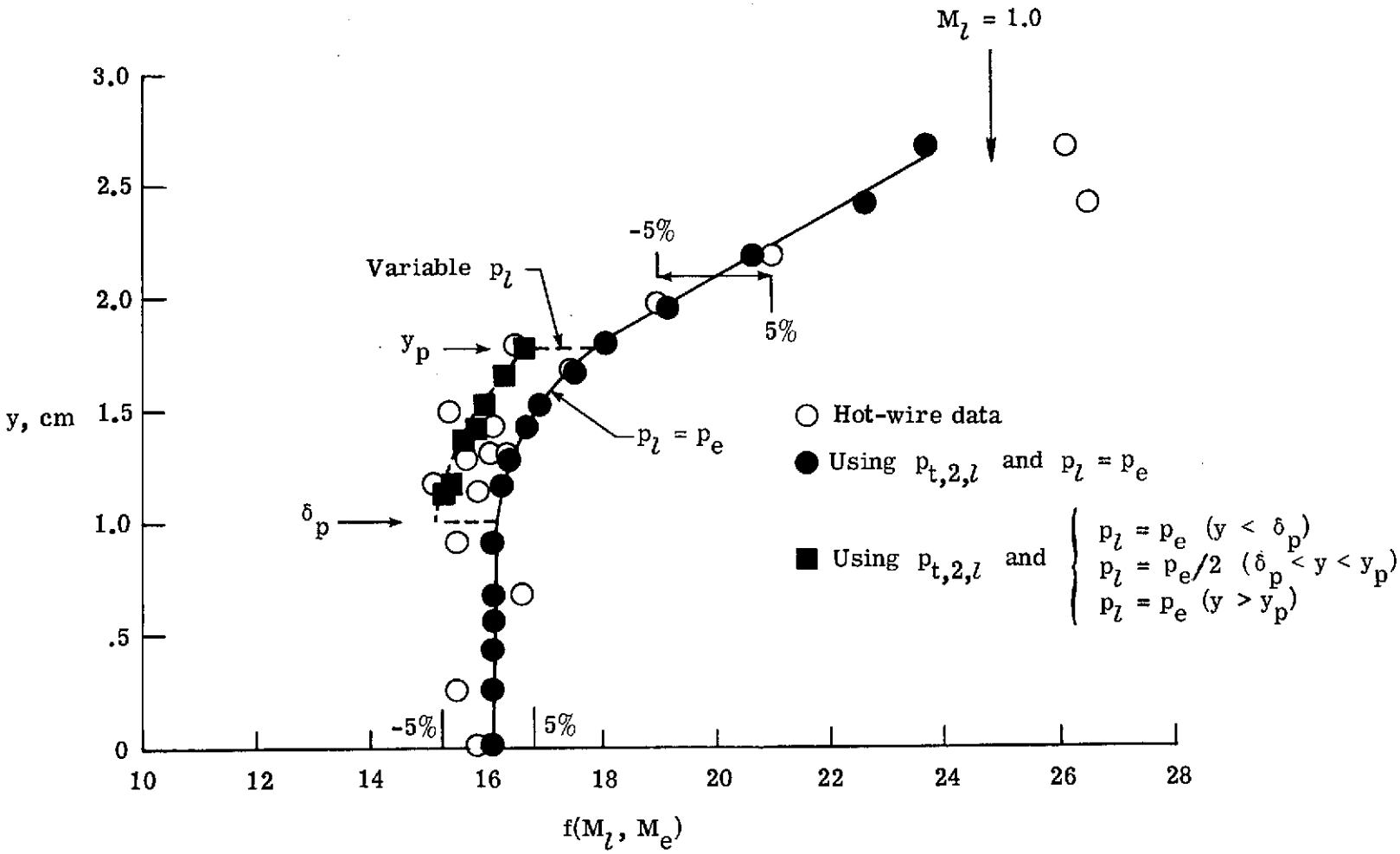

Figure 6.- Mean flow determination.

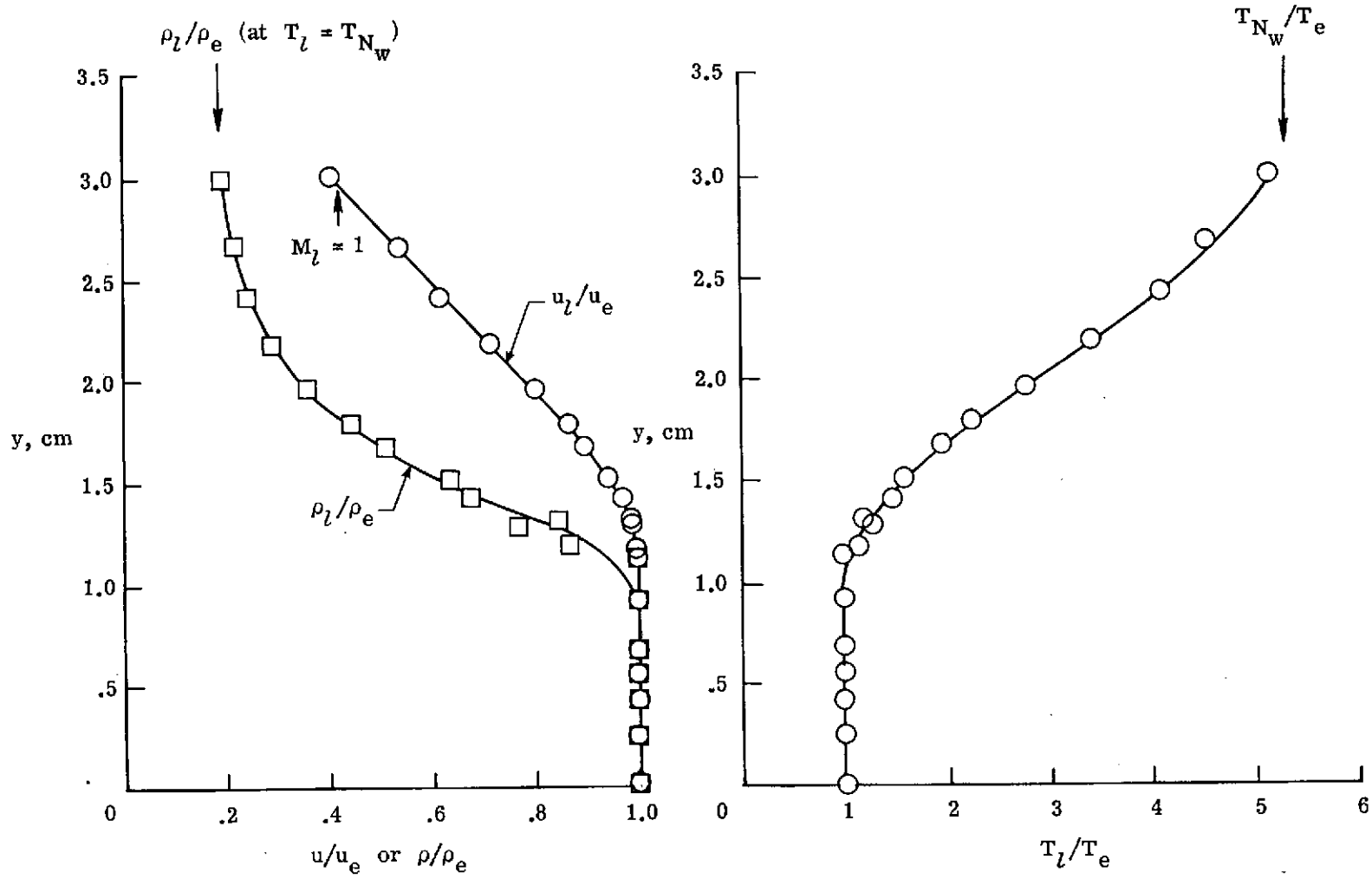

Figure 7.- Mean flow profiles.

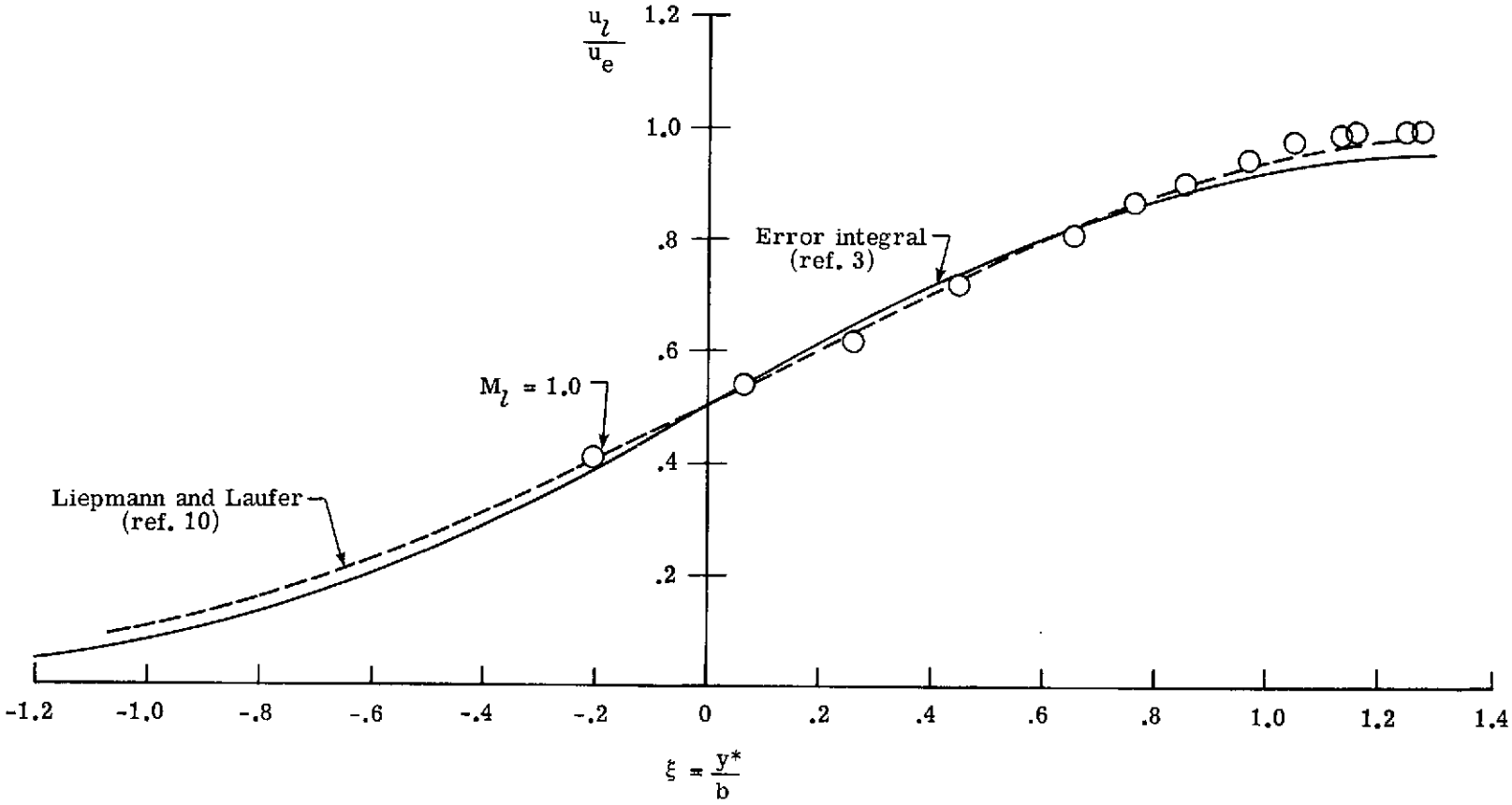

Figure 8.- Comparison of subsonic and supersonic velocity profiles.

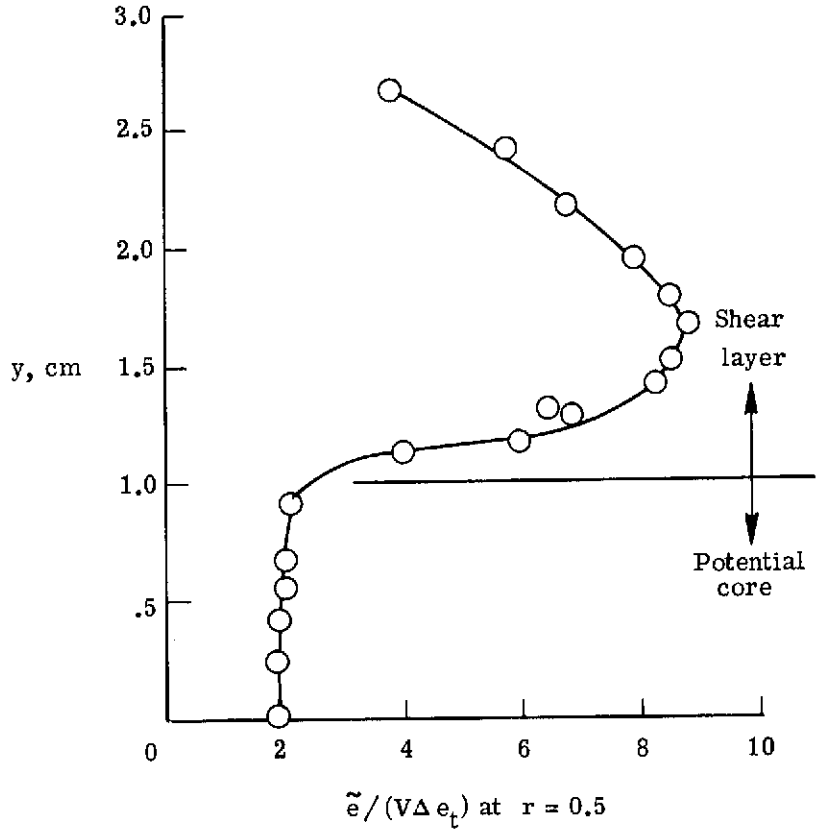

Figure 9.- Virtual total-temperature fluctuations through shear layer and potential core at x = 26.7 cm.

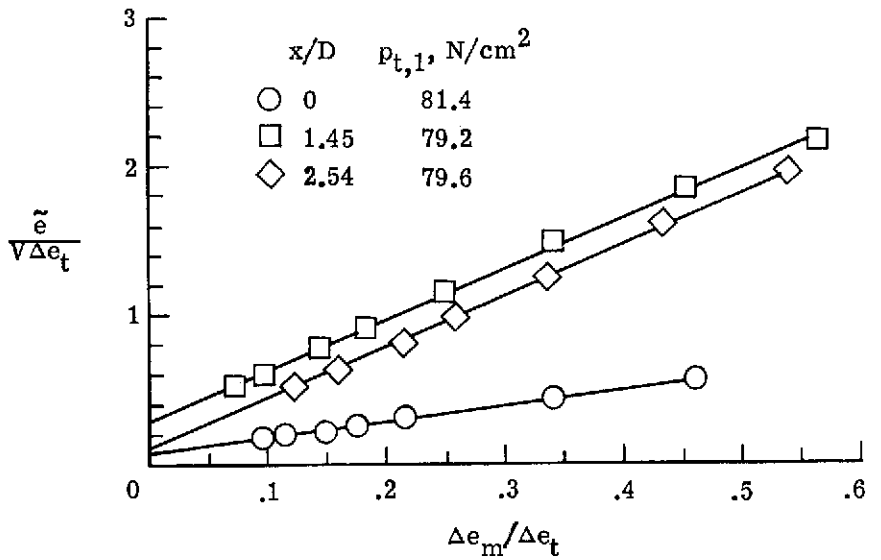

Figure 10.- Hot-wire mode diagrams in potential core.

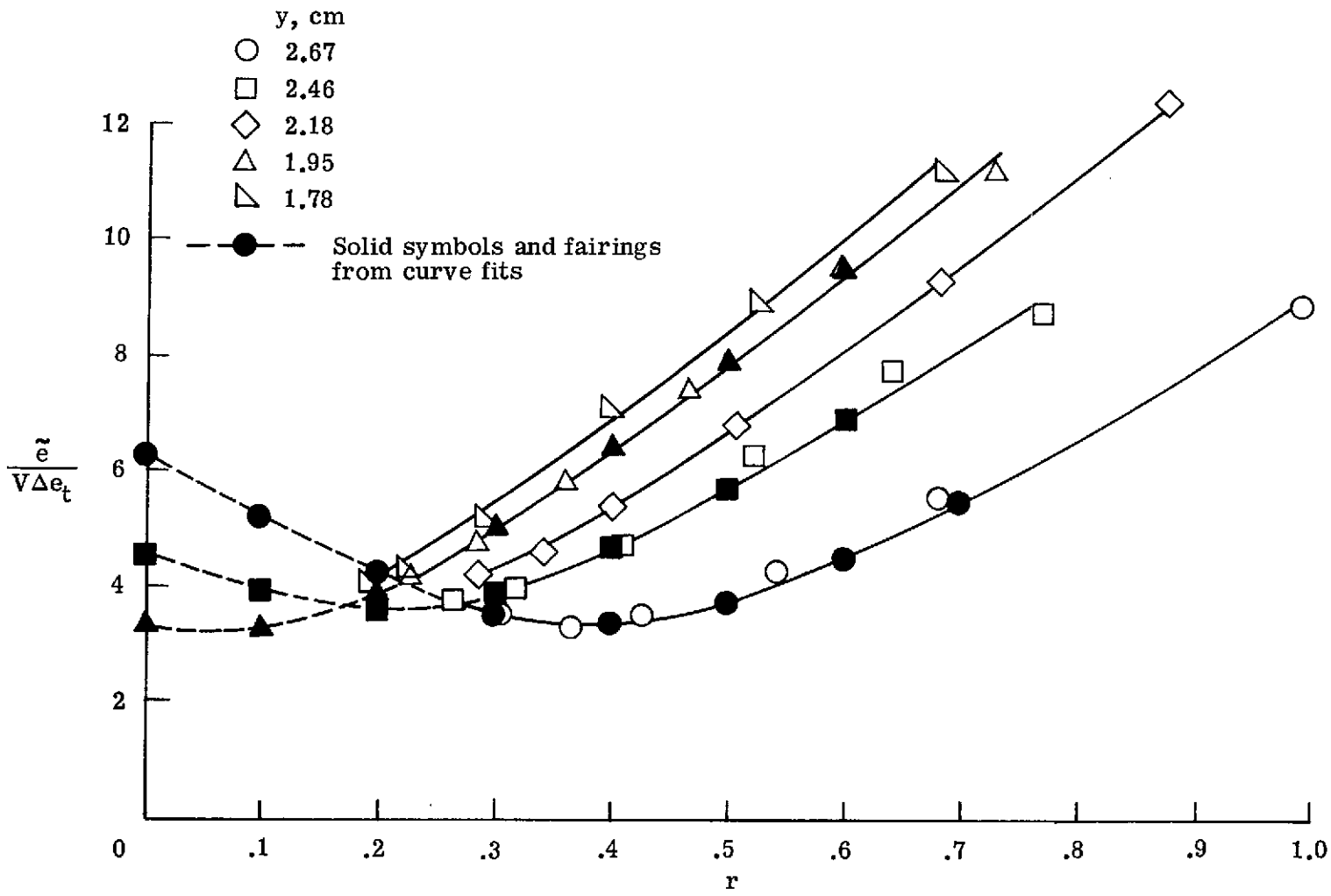

Figure 11.- Mode diagrams; x = 26.7 cm.

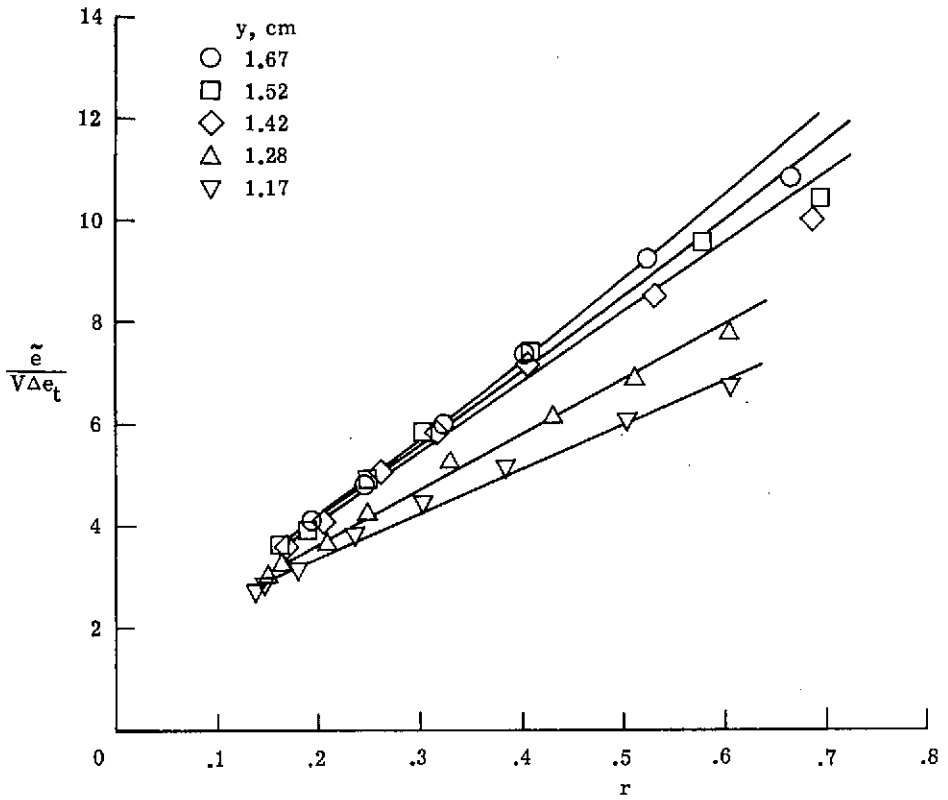

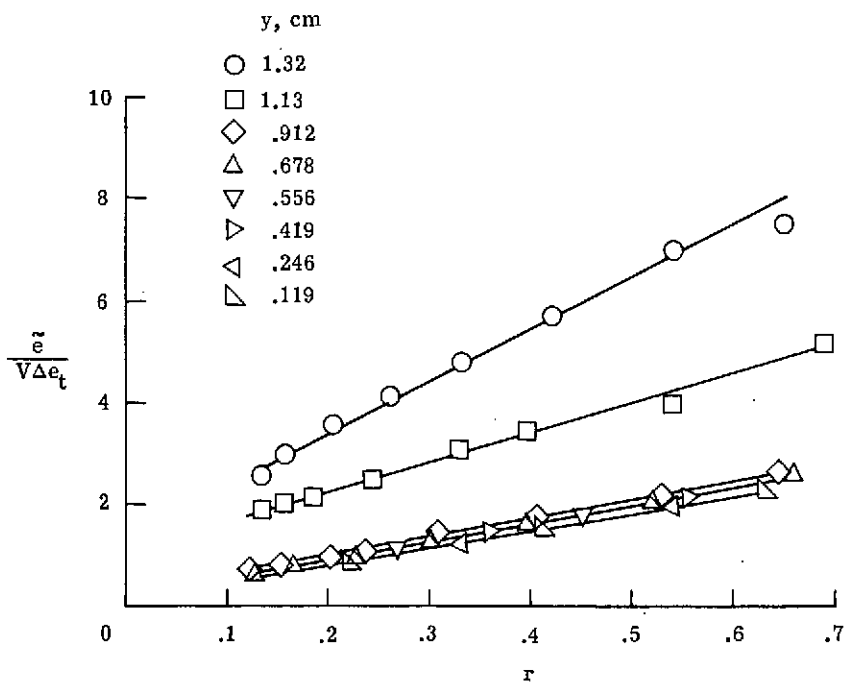

Figure 11.- Concluded.

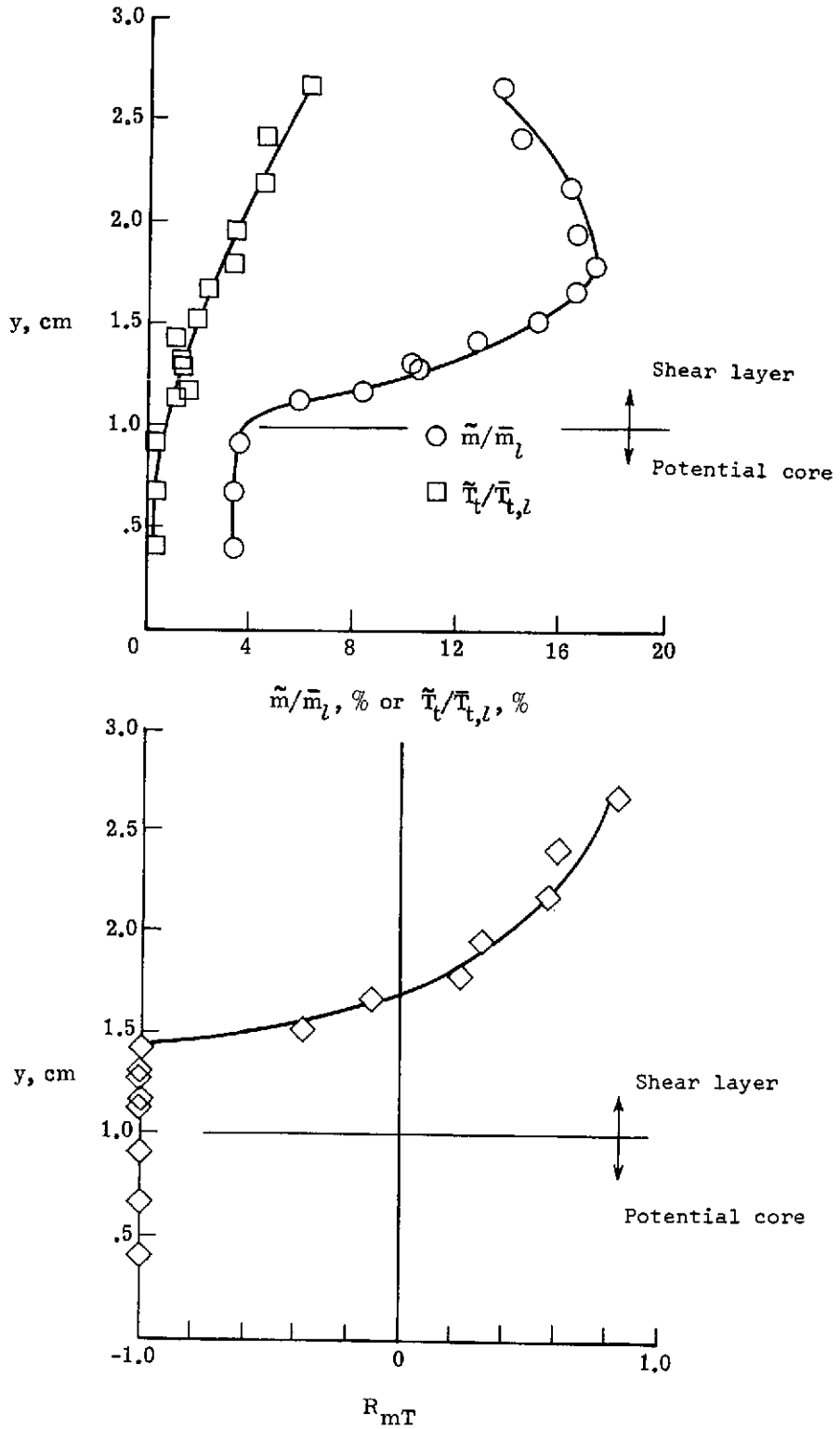

Figure 12.- Root mean square of mass flow and total-temperature fluctuations and correlation coefficient.

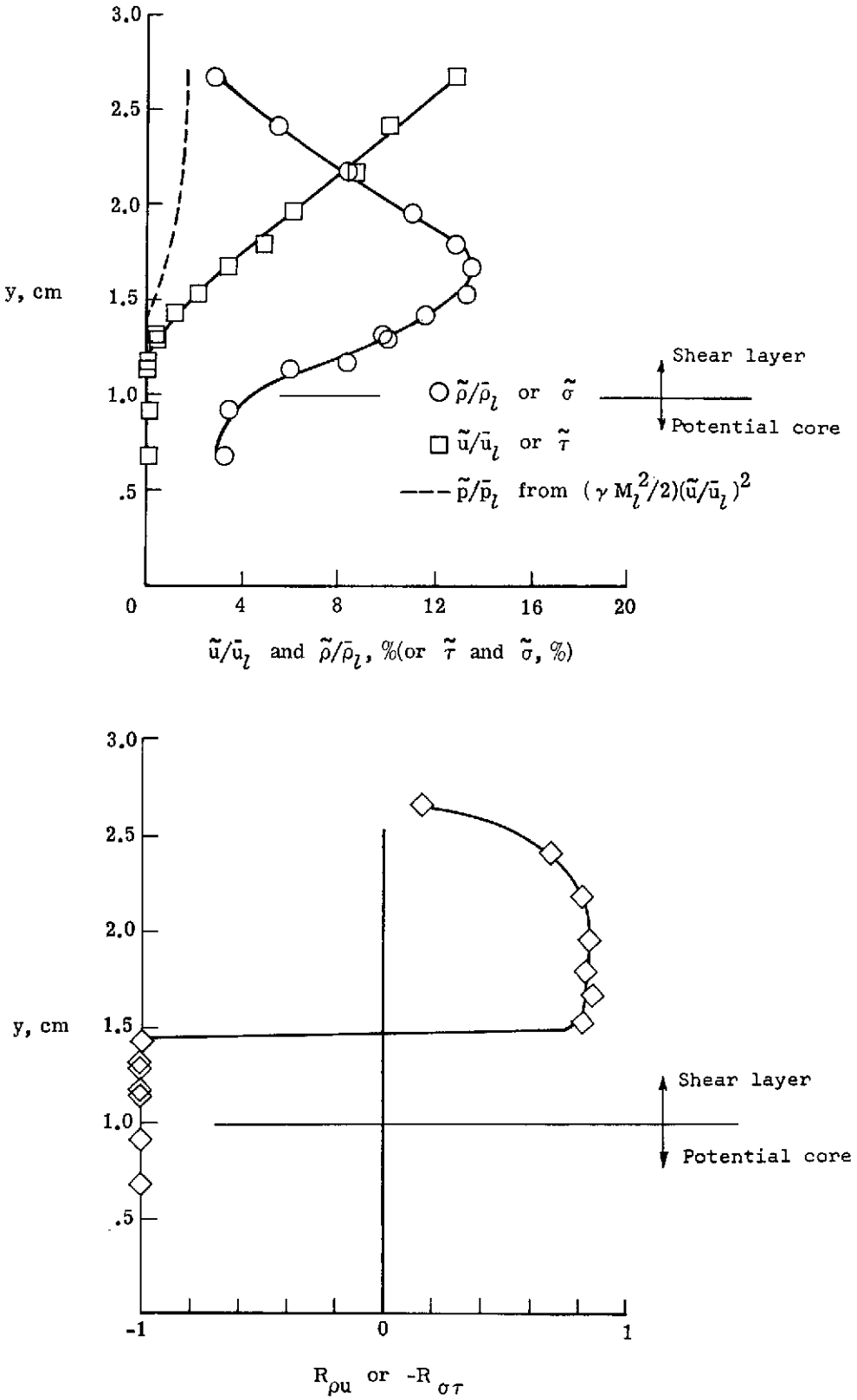

Figure 13.- Velocity and density fluctuations and $R_{\rho u}$.

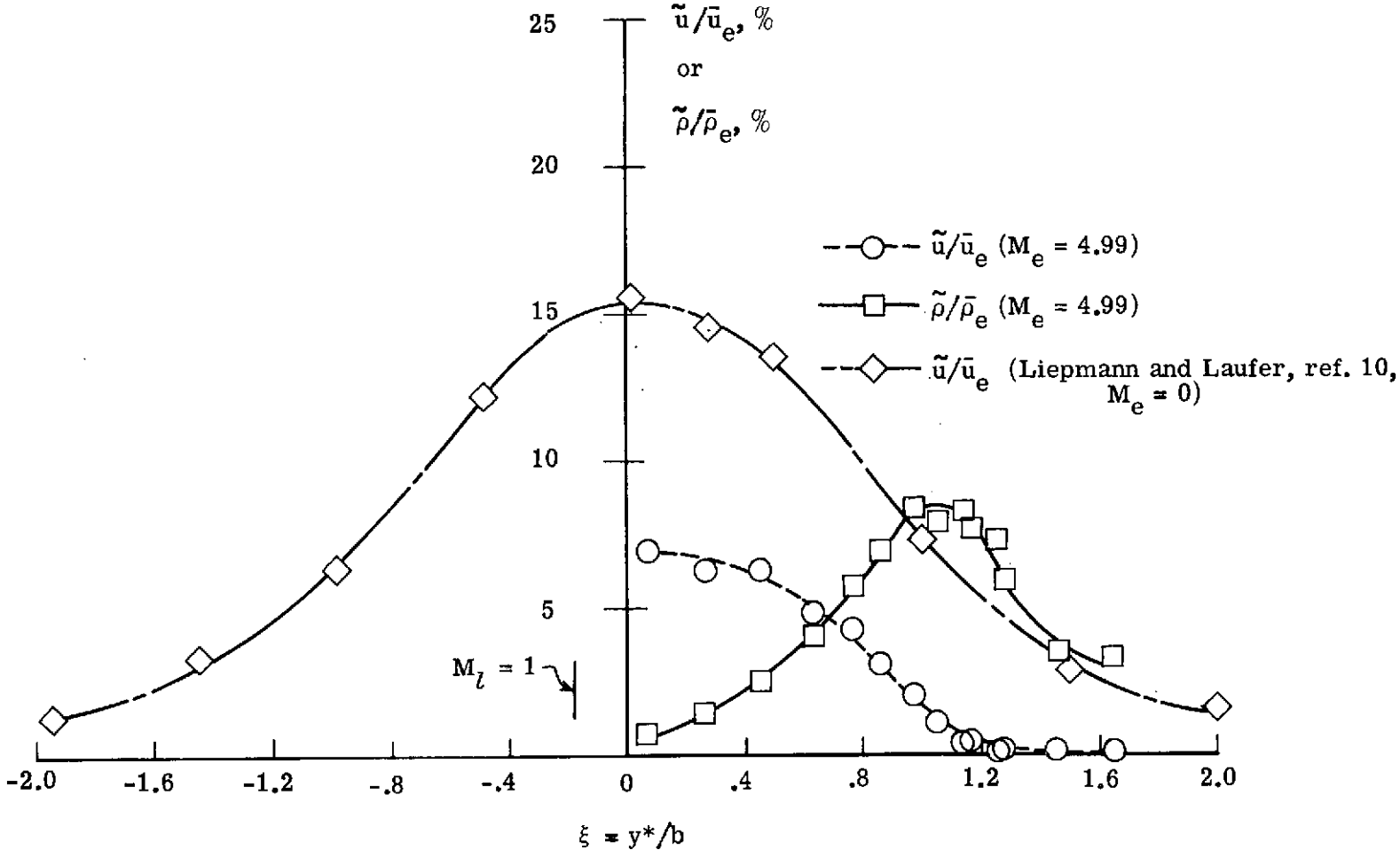

Figure 14.- Comparison of subsonic and hypersonic results.

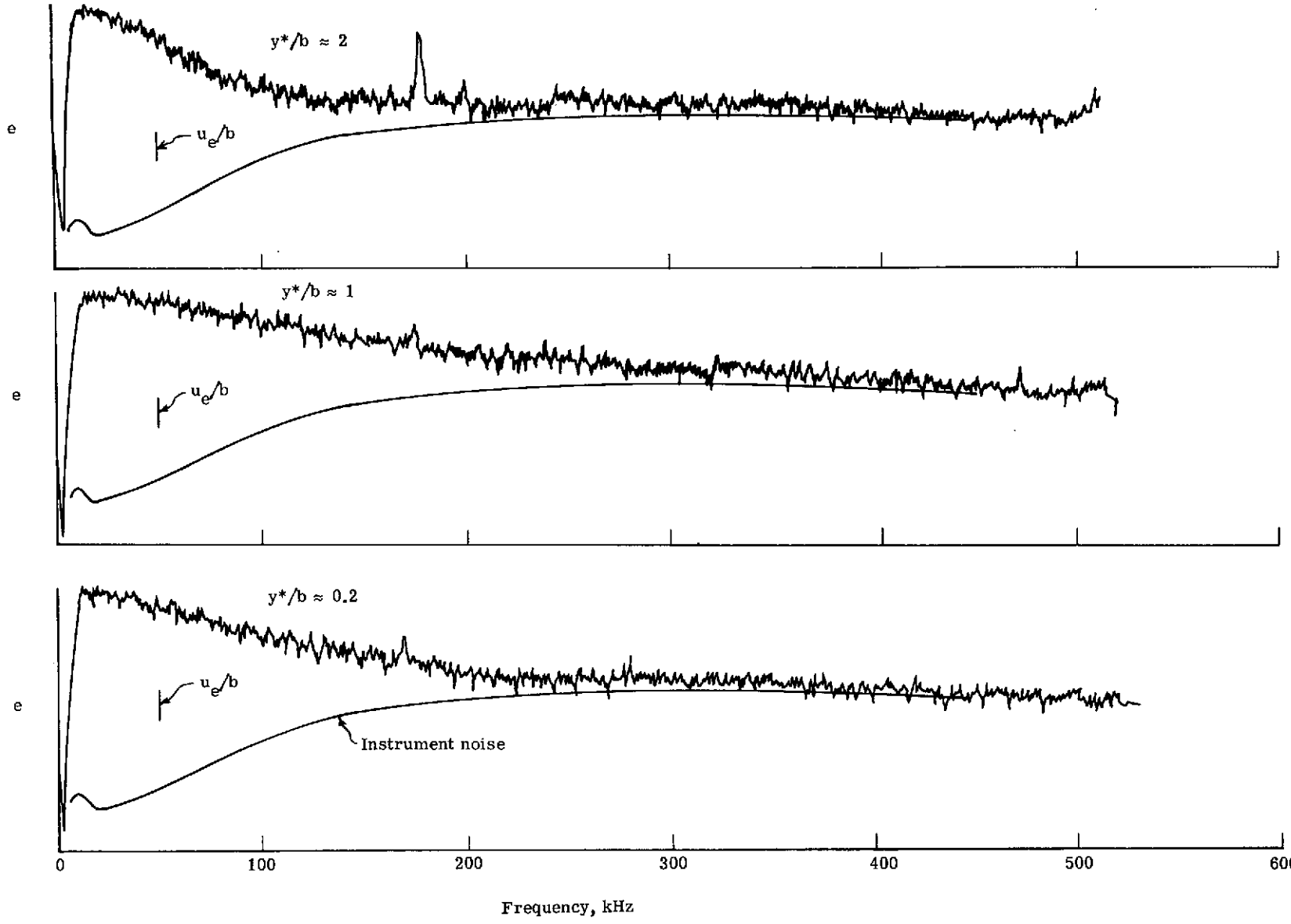

Figure 15.- Hot-wire signal spectra.